SIAM J. APPL. MATH.
Vol. 76, No. 2, pp. 598–617

A NORMAL FORM FOR HAMILTONIAN–HOPF BIFURCATIONS IN NONLINEAR SCHRÖDINGER EQUATIONS WITH GENERAL EXTERNAL POTENTIALS*

JIANKE YANG†

Abstract. A normal form is derived for Hamiltonian–Hopf bifurcations of solitary waves in nonlinear Schrödinger equations with general external potentials. This normal form is a simple second-order nonlinear ordinary differential equation (ODE) that is asymptotically accurate in describing solution dynamics near Hamiltonian–Hopf bifurcations. When the nonlinear coefficient in this normal form is complex, which occurs if the second harmonic of the Hopf bifurcation frequency falls inside the continuous spectrum of the system, the solution of this normal form will blow up to infinity in finite time, meaning that solution oscillations near Hamiltonian–Hopf bifurcations will strongly amplify and eventually be destroyed. When the nonlinear coefficient of the normal form is real, the normal form can admit periodic solutions, which correspond to long-lasting solution oscillations in the original partial differential equation (PDE) system. Quantitative comparison between the normal form's predictions and true PDE solutions is also made in several numerical examples, and good agreement is obtained.

Key words. Hamiltonian–Hopf bifurcation, normal form, nonlinear Schrödinger equation, external potential

AMS subject classifications. 35Q55, 35Q60

DOI. 10.1137/15M1042619

1. Introduction.

Bifurcations of stationary waves are common phenomena in both conservative and dissipative nonlinear wave systems (see, for instance, [1, 2, 3, 4, 5, 6, 7, 8, 9, 10, 11, 12, 13, 14, 15, 16, 17, 18, 19, 20]). Notable examples include symmetry-breaking bifurcations, fold bifurcations, Hopf bifurcations, and period-doubling bifurcations, all of which have counterparts in dynamical systems. Bifurcations of stationary waves induce qualitative changes to the wave behavior and can be used to control system outcome, and thus their study is both mathematically and physically important.

Hamiltonian–Hopf bifurcations occur in conservative wave systems, where pairs of imaginary eigenvalues in the linear-stability spectrum of stationary waves coalesce and then move off the imaginary axis, creating oscillatory instability. These linear instabilities have been well analyzed, and it has been shown that only collisions of imaginary eigenvalues with opposite Krein signatures can induce such bifurcations [21, 22, 23]. However, nonlinear wave dynamics near such bifurcations is less known. One step in this direction was made by Goodman [15], where Hamiltonian–Hopf bifurcations of solitary waves were examined in the nonlinear Schrödinger (NLS) equation with potentials of primarily symmetric triple-well type. Projecting the solution to three linear eigenmodes of the potential and making a Galerkin truncation and symmetry reduction, a Hamiltonian system of ordinary differential equations (ODEs) for two complex variables was derived. Numerical simulations of this ODE model showed

*Received by the editors October 5, 2015; accepted for publication (in revised form) January 4, 2016; published electronically March 17, 2016. This work was supported in part by the Air Force Office of Scientific Research (grant USAF 9550-12-1-0244) and the National Science Foundation (grant DMS-1311730).

http://www.siam.org/journals/siap/76-2/M104261.html

†Department of Mathematics and Statistics, University of Vermont, Burlington, VT 05401 (jyang@math.uvm.edu).

oscillatory as well as chaotic solutions at different power levels, which resemble dynamics in the original partial differential equation (PDE) system. However, this analysis is suitable only for Hamiltonian–Hopf bifurcations at low powers of solitons, where the solution projection onto linear modes is justified (at higher soliton powers, the error of Galerkin truncation will be significant). In addition, the derived ODE model is complicated, which hinders analytical predictions of ODE dynamics. Furthermore, the resonant effect of higher harmonics of solution oscillations with the continuous spectrum is invisible in this analysis.

In this paper, we derive a normal form for general Hamiltonian–Hopf bifurcations of solitary waves (solitons) in NLS equations with arbitrary external potentials. This normal form is a simple second-order nonlinear ODE. It is derived near a Hamiltonian–Hopf bifurcation point by multiscale perturbation methods and is asymptotically accurate in describing solution dynamics near Hamiltonian–Hopf bifurcations (here asymptotic accuracy means that the normal form's prediction will be quantitatively more accurate if the initial condition of the PDE is closer to the soliton at the Hamiltonian–Hopf bifurcation point). When the nonlinear coefficient in this normal form is complex, which occurs if the second harmonic of the Hopf bifurcation frequency is resonant with the continuous spectrum of the system, the solution of this normal form will blow up to infinity in finite time, meaning that solution oscillations near Hamiltonian–Hopf bifurcations will strongly amplify and eventually be destroyed. When the nonlinear coefficient of the normal form is real, the normal form can admit periodic solutions, which correspond to long-lasting solution oscillations in the original PDE system. Quantitative comparison between the normal form's predictions and true PDE solutions is also made in several numerical examples, and good agreement is obtained.

2. Analytical conditions for Hamiltonian–Hopf bifurcations. We consider the NLS equation with a general external localized potential,

$$iU_t + U_{xx} - V(x)U + \sigma|U|^2U = 0, \tag{2.1}$$

where $V(x)$ is a real-valued potential function which decays to zero at infinity (with any decay rate), and $\sigma = \pm 1$ is the sign of nonlinearity. This equation models not only nonlinear light propagation in a Kerr medium under paraxial approximation but also dynamics of Bose–Einstein condensates under mean-field approximation (in the latter community, this equation is referred to as the Gross–Pitaevskii equation) [24, 25, 26]. Equation (2.1) is a Hamiltonian system. Note that the cubic nonlinearity and localized linear potential in this model are chosen primarily for convenience, as the analysis to be developed in this paper can be readily extended to arbitrary forms of nonlinearities and potentials [19].

Solitons in (2.1) have the form

$$U(x,t) = e^{i\mu t}u(x), \tag{2.2}$$

where $u(x)$ is a real-valued localized function solving the equation

$$u_{xx} - \mu u - V(x)u + \sigma u^3 = 0, \tag{2.3}$$

and μ is a real-valued propagation constant. These solitons exist as continuous families parameterized by μ, and it is assumed that the solitons are differentiable with respect to μ. Since the potential $V(x)$ is localized, μ is positive for all these solitons.

Linear stability of these solitons is determined by substituting the normal-mode perturbation

$$U(x,t) = e^{i\mu t}\left[u(x) + f_1(x)e^{\lambda t} + f_2^*(x)e^{\lambda^* t}\right], \quad f_1, f_2 \ll 1, \tag{2.4}$$

into (2.1), which leads to the linear eigenvalue problem

$$iL\begin{bmatrix} f_1 \\ f_2 \end{bmatrix} = \lambda \begin{bmatrix} f_1 \\ f_2 \end{bmatrix}, \tag{2.5}$$

where

$$L = \begin{bmatrix} \partial_{xx} - \mu - V + 2\sigma u^2 & \sigma u^2 \\ -\sigma u^2 & -(\partial_{xx} - \mu - V + 2\sigma u^2) \end{bmatrix}, \tag{2.6}$$

λ is the eigenvalue, and the superscript * represents complex conjugation. Notice that $\sigma_3 L$ is a self-adjoint operator, where $\sigma_3 = \mathrm{diag}(1,-1)$ is the third Pauli-spin matrix. That is, $(\sigma_3 L)^A = \sigma_3 L$, with the superscript A representing the adjoint of an operator (in the square-integrable functional space). Thus

$$L^A = \sigma_3 L \sigma_3. \tag{2.7}$$

It is easy to see that if λ is an eigenvalue of iL, so are λ^*, $-\lambda$, and $-\lambda^*$. Thus purely real and purely imaginary eigenvalues appear as $\pm\lambda$ pairs, and other eigenvalues appear as quadruples. If all eigenvalues λ lie on the imaginary axis, then the soliton (2.2) is spectrally stable; otherwise it is spectrally unstable.

Hamiltonian–Hopf bifurcations of solitons occur when pairs of discrete eigenvalues on the imaginary axis collide and move off the imaginary axis, creating linear oscillatory instability. Here discrete eigenvalues refer to eigenvalues whose eigenfunctions are square-integrable. Suppose this Hamiltonian–Hopf bifurcation occurs at the soliton $u_0(x)$ with $\mu = \mu_0 > 0$, eigenvalues collide at $\lambda = \pm i\omega$ on the imaginary axis (with $\omega > 0$ being the Hopf frequency), and $i\omega$ is a double discrete eigenvalue of iL_0, where $L_0 \equiv L|_{\mu=\mu_0}$. Then the condition for this bifurcation is that the geometric multiplicity of $i\omega$ is one (less than its algebraic multiplicity two). In other words, the double eigenvalue $i\omega$ of iL_0 admits a single eigenfunction and a generalized eigenfunction. More explicitly, there exist a single real eigenfunction $[\psi_1, \psi_2]^T$ and a generalized real eigenfunction $[\phi_1, \phi_2]^T$ such that

$$L_0\begin{bmatrix} \psi_1 \\ \psi_2 \end{bmatrix} = \omega \begin{bmatrix} \psi_1 \\ \psi_2 \end{bmatrix}, \tag{2.8}$$

$$(L_0 - \omega)\begin{bmatrix} \phi_1 \\ \phi_2 \end{bmatrix} = \begin{bmatrix} \psi_1 \\ \psi_2 \end{bmatrix}, \tag{2.9}$$

and no higher generalized eigenfunctions exist; i.e., the equation

$$(L_0 - \omega)\begin{bmatrix} \chi_1 \\ \chi_2 \end{bmatrix} = \begin{bmatrix} \phi_1 \\ \phi_2 \end{bmatrix} \tag{2.10}$$

admits no solutions (in the square-integrable functional space). Here the superscript T represents transpose of a vector. In view of (2.7), we see that

$$(L_0 - \omega)^A \begin{bmatrix} \psi_1 \\ -\psi_2 \end{bmatrix} = 0, \tag{2.11}$$

i.e., $[\psi_1, -\psi_2]^T$ is in the kernel of $(L_0 - \omega)^A$. Hence, in order for the generalized eigenfunction $[\phi_1, \phi_2]^T$ to exist in (2.9), the right-hand side of this linear inhomogeneous equation must be orthogonal to the adjoint homogeneous solution $[\psi_1, -\psi_2]^T$, i.e.,

$$\int_{-\infty}^{\infty} (\psi_1^2 - \psi_2^2) dx = 0, \tag{2.12}$$

and in order for higher generalized eigenfunctions not to exist in (2.10), the right-hand side of (2.10) must not be orthogonal to $[\psi_1, -\psi_2]^T$, i.e.,

$$\int_{-\infty}^{\infty} (\psi_1 \phi_1 - \psi_2 \phi_2) dx \neq 0. \tag{2.13}$$

Necessary conditions for Hamiltonian–Hopf bifurcations can also be formulated using Krein signatures of purely imaginary discrete eigenvalues in the linear-stability operator iL [21, 23]. For a simple purely imaginary discrete eigenvalue $\lambda = i\omega$ with real eigenfunction $F = [f_1, f_2]^T$, its Krein signature can be defined as

$$K_\lambda = \text{sgn}\langle -\sigma_3 L F, F\rangle = \text{sgn} \int_{-\infty}^{\infty} \omega (f_2^2 - f_1^2) dx, \tag{2.14}$$

where the inner product between two vector functions $f(x)$ and $g(x)$ is $\langle f, g\rangle = \int_{-\infty}^{\infty} f^{*T} g \, dx$. When two such eigenvalues collide on the imaginary axis, a necessary condition for Hamiltonian–Hopf bifurcations is that they have opposite Krein signatures [21, 23]. This necessary condition on Krein signatures is related to the conditions on eigenfunctions given above. Indeed, under conditions (2.12)–(2.13) for eigenfunctions, we can show that the purely imaginary eigenvalues before collision have opposite Krein signatures (details are omitted).

Regarding the operator L_0, it should be said that zero is its discrete eigenvalue since

$$L_0 \begin{bmatrix} u_0 \\ -u_0 \end{bmatrix} = 0. \tag{2.15}$$

Similarly, zero is a discrete eigenvalue of L_0^A since

$$L_0^A \begin{bmatrix} u_0 \\ u_0 \end{bmatrix} = 0 \tag{2.16}$$

in view of (2.7). In addition, by differentiating the soliton equation (2.3) with respect to μ, we get

$$L_0 \begin{bmatrix} u_{\mu 0} \\ u_{\mu 0} \end{bmatrix} = \begin{bmatrix} u_0 \\ -u_0 \end{bmatrix}, \tag{2.17}$$

where $u_{\mu 0}(x) \equiv u_\mu(x;\mu)|_{\mu=\mu_0}$. Furthermore, since the potential $V(x)$ and the soliton $u_0(x)$ are both localized, the continuous spectrum of iL_0 is $i(-\infty, -\mu_0] \bigcup i[\mu_0, +\infty)$ on the imaginary axis. These facts will be used in later analysis.

In the next section, we will investigate solution dynamics near Hamiltonian–Hopf bifurcations. For that purpose, we make the following additional assumptions:

1. $2i\omega$ is not a discrete eigenvalue of iL_0.

2. Defining the linearization operator of the soliton equation (2.3) at $\mu = \mu_0$ (in the square-integrable functional space) as

$$M = \partial_{xx} - \mu_0 - V(x) + 3\sigma u_0^2, \tag{2.18}$$

we assume that the kernel of M is empty.

3. Defining the power of solitons $u(x;\mu)$ as

$$P(\mu) = \int_{-\infty}^{\infty} u^2(x;\mu)dx, \tag{2.19}$$

we assume that $P'(\mu_0) \neq 0$.

The first assumption forbids nonlinearity-induced second-harmonic resonance of Hopf–bifurcation eigenmodes, the second prohibits other potential bifurcations of solitons at this Hamiltonian–Hopf bifurcation point [19], and the third excludes additional linear instabilities [26]. These assumptions will be needed for our analysis.

3. A normal form for Hamiltonian–Hopf bifurcations. In this section, we derive an asymptotically accurate ODE model (a normal form) for wave dynamics near Hamiltonian–Hopf bifurcations. This normal form uses only information at the bifurcation point.

Near a Hamiltonian–Hopf bifurcation point $\mu = \mu_0$, we assume that the full PDE solution can be expanded into the perturbation series

$$U(x,t) = e^{i\theta}\left[u_0(x) + \epsilon U_1(x,t,T) + \epsilon^2 U_2(x,t,T) + \cdots\right], \tag{3.1}$$

where

$$\theta(t,T) = \mu_0 t + \epsilon \int_0^T \mu_1(\widehat{T})\, d\widehat{T} + \epsilon^2 \int_0^T \mu_2(\widehat{T})\, d\widehat{T} + \cdots, \tag{3.2}$$

$T = \epsilon t$, and $0 < \epsilon \ll 1$ is a small parameter which measures the deviation of this solution from the soliton $u_0(x)$. Substituting this expansion into (2.1), the $O(1)$ equation is automatically satisfied. At $O(\epsilon)$, the equation for U_1 is found to be

$$(i\partial_t + \partial_{xx} - \mu_0 - V + 2\sigma u_0^2)U_1 + \sigma u_0^2 U_1^* = 0. \tag{3.3}$$

This equation can be rewritten as

$$(i\partial_t + L_0)\begin{bmatrix} U_1 \\ U_1^* \end{bmatrix} = 0. \tag{3.4}$$

In view of the conditions for Hamiltonian–Hopf bifurcations in section 2, $i\omega$ is a double eigenvalue of iL_0 with a single real eigenfunction $[\psi_1, \psi_2]^T$. Due to eigenvalue symmetry, $-i\omega$ is also a double eigenvalue of iL_0 with a single real eigenfunction $[\psi_2, \psi_1]^T$. Thus the nonsecular localized solution for U_1 is a slowly modulated Hopf oscillation mode

$$U_1 = B(T)\psi_1(x)e^{i\omega t} + B^*(T)\psi_2(x)e^{-i\omega t}, \tag{3.5}$$

where $B(T)$ is a complex envelope function to be determined.

At $O(\epsilon^2)$, the equation for U_2 is

$$\begin{aligned}&(i\partial_t + \partial_{xx} - \mu_0 - V + 2\sigma u_0^2)U_2 + \sigma u_0^2 U_2^* \\ &\quad = \mu_1 u_0 - iU_{1T} - \sigma u_0\left(2|U_1|^2 + U_1^2\right).\end{aligned} \tag{3.6}$$

When the U_1 formula (3.5) is utilized, this U_2 equation becomes

$$\begin{aligned}(i\partial_t + \partial_{xx} - \mu_0 - V + 2\sigma u_0^2)U_2 + \sigma u_0^2 U_2^* &= \mu_1 u_0 \\ -2\sigma|B|^2 u_0(\psi_1^2 + \psi_1\psi_2 + \psi_2^2) - iB_T\psi_1 e^{i\omega t} - iB_T^*\psi_2 e^{-i\omega t} &\\ -\sigma B^2 u_0(2\psi_1\psi_2 + \psi_1^2)e^{2i\omega t} - \sigma B^{*2} u_0(2\psi_1\psi_2 + \psi_2^2)e^{-2i\omega t}. &\end{aligned} \tag{3.7}$$

In view of (2.9) and (2.17), the solution to this U_2 equation is

$$\begin{aligned}U_2 = \mu_1 u_{\mu 0} - \sigma|B|^2 h - iB_T\phi_1 e^{i\omega t} + iB_T^*\phi_2 e^{-i\omega t} &\\ -\sigma B^2 g_1 e^{2i\omega t} - \sigma B^{*2} g_2^* e^{-2i\omega t}, &\end{aligned} \tag{3.8}$$

where $h(x)$ is a real localized function defined by

$$h = M^{-1}\left[2u_0(\psi_1^2 + \psi_1\psi_2 + \psi_2^2)\right], \tag{3.9}$$

$[\phi_1(x), \phi_2(x)]^T$ is the real generalized eigenfunction defined in (2.9), and $[g_1(x), g_2(x)]^T$ solves the equation

$$(L_0 - 2\omega)\begin{bmatrix} g_1 \\ g_2 \end{bmatrix} = \begin{bmatrix} u_0(2\psi_1\psi_2 + \psi_1^2) \\ -u_0(2\psi_1\psi_2 + \psi_2^2) \end{bmatrix}. \tag{3.10}$$

Note that the kernel of M is empty due to our second assumption at the end of section 2; thus a localized real function $h(x)$ as defined in (3.9) exists and is unique.

The following important remarks are in order regarding the nature of the solution $[g_1, g_2]^T$ to (3.10), and this hinges on whether $2i\omega$ lies inside the continuous spectrum $i(-\infty, -\mu_0]\bigcup i[\mu_0, +\infty)$ of the linear-stability operator iL_0.

(1) If $2i\omega$ does not lie in this continuous spectrum, meaning that $2\omega < \mu_0$, then in view of our first assumption at the end of section 2, the kernel of $L_0 - 2\omega$ is empty, and thus a localized real solution $[g_1, g_2]^T$ to (3.10) exists and is unique.

(2) If $2i\omega$ lies inside the continuous spectrum of iL_0, i.e., $2\omega > \mu_0$, then resonance with the continuous spectrum occurs. In this case, the forcing term on the right-hand side of (3.10) will excite continuous-wave radiation, which appears in the g_2 component. This radiation must spread from the central region to the far field, i.e., it must satisfy the Sommerfeld radiation condition

$$\begin{bmatrix} g_1 \\ g_2 \end{bmatrix} \to \begin{cases} \begin{bmatrix} 0 \\ R_+ e^{-ikx} \end{bmatrix}, & x \gg 1, \\ \begin{bmatrix} 0 \\ R_- e^{ikx} \end{bmatrix}, & x \ll -1, \end{cases} \tag{3.11}$$

where $k = \sqrt{2\omega - \mu_0}$ is the wavenumber of large-x radiation with frequency 2ω, and $R_\pm$ are constants which measure the radiation amplitudes at large-x. A consequence of the Sommerfeld radiation condition is that the resulting solution $[g_1, g_2]^T$ is complex and nonlocal, and this solution can be uniquely determined by various methods [26, 27].

After the U_2 solution (3.8) is obtained, we now proceed to the U_3 equation at order ϵ^3. This U_3 equation is

$$\begin{aligned}(i\partial_t + \partial_{xx} - \mu_0 - V + 2\sigma u_0^2)U_3 + \sigma u_0^2 U_3^* &\\ = \mu_1 U_1 + \mu_2 u_0 - iU_{2T} &\\ -\sigma\left(2u_0 U_1 U_2 + 2u_0 U_1^* U_2 + 2u_0 U_1 U_2^* + |U_1|^2 U_1\right). &\end{aligned} \tag{3.12}$$

Inserting the U_1 and U_2 formulae (3.5) and (3.8), this U_3 equation reduces to

$$\begin{aligned}(i\partial_t+\partial_{xx}-\mu_0-V+2\sigma u_0^2)U_3+\sigma u_0^2U_3^*\\ =Q_0+Q_1e^{i\omega t}+Q_2^*e^{-i\omega t}+Q_3e^{2i\omega t}+Q_4^*e^{-2i\omega t}\\ +Q_5e^{3i\omega t}+Q_6^*e^{-3i\omega t},\end{aligned}\tag{3.13}$$

where

$$\begin{aligned}Q_0=-i\left[\mu_{1T}u_{\mu 0}-\sigma h(|B|^2)_T\right]\\ -2\sigma u_0\left[iBB_T^*(\psi_1\phi_1+\psi_2\phi_2+\psi_1\phi_2)\right.\\ \left.-iB^*B_T(\psi_1\phi_1+\psi_2\phi_2+\psi_2\phi_1)\right],\end{aligned}\tag{3.14}$$

$$\begin{aligned}Q_1=\mu_1B\left[\psi_1-2\sigma u_0u_{\mu 0}(2\psi_1+\psi_2)\right]-B_{TT}\phi_1\\ -\sigma|B|^2B\left[\psi_1(2\psi_2^2+\psi_1^2)-2\sigma u_0h(2\psi_1+\psi_2)\right.\\ \left.-2\sigma u_0(\psi_1g_1+\psi_2g_1+\psi_2g_2)\right],\end{aligned}\tag{3.15}$$

$$\begin{aligned}Q_2=\mu_1B\left[\psi_2-2\sigma u_0u_{\mu 0}(2\psi_2+\psi_1)\right]+B_{TT}\phi_2\\ -\sigma|B|^2B\left[\psi_2(2\psi_1^2+\psi_2^2)-2\sigma u_0h(2\psi_2+\psi_1)\right.\\ \left.-2\sigma u_0(\psi_1g_1+\psi_1g_2+\psi_2g_2)\right],\end{aligned}\tag{3.16}$$

and Q_3, Q_4, Q_5, Q_6 are functions that are unimportant in our analysis and thus not shown here. This U_3 solution can be decomposed as

$$\begin{aligned}U_3(x,t)=U_{30}+U_{31}e^{i\omega t}+U_{32}^*e^{-i\omega t}\\ +U_{33}e^{2i\omega t}+U_{34}^*e^{-2i\omega t}+U_{35}e^{3i\omega t}+U_{36}^*e^{-3i\omega t},\end{aligned}\tag{3.17}$$

where

$$L_0\begin{bmatrix}U_{30}\\ U_{30}^*\end{bmatrix}=\begin{bmatrix}Q_0\\ -Q_0^*\end{bmatrix}\tag{3.18}$$

and

$$(L_0-\omega)\begin{bmatrix}U_{31}\\ U_{32}\end{bmatrix}=\begin{bmatrix}Q_1\\ -Q_2\end{bmatrix}.\tag{3.19}$$

The Fredholm solvability conditions of the above two equations are that their inhomogeneous terms on the right-hand sides be orthogonal to the localized adjoint homogeneous solutions. In view of (2.11) and (2.16), these solvability conditions are

$$\int_{-\infty}^{\infty}u_0(Q_0-Q_0^*)dx=0\tag{3.20}$$

and

$$\int_{-\infty}^{\infty}(\psi_1Q_1+\psi_2Q_2)\,dx=0.\tag{3.21}$$

Inserting the expressions of Q_0, Q_1, and Q_2 above, these solvability conditions lead to the following dynamical equations for the slow variables $\mu_1(T)$ and $B(T)$:

$$\mu_{1T}=\alpha(|B|^2)_T,\tag{3.22}$$

$$B_{TT}-\beta\mu_1B+\gamma|B|^2B=0,\tag{3.23}$$

where

$$\alpha = \frac{2\sigma}{P'(\mu_0)} \int_{-\infty}^{\infty} u_0 \left[h - u_0(\psi_1\phi_2 - \psi_2\phi_1)\right] dx, \tag{3.24}$$

$$\beta = \frac{\int_{-\infty}^{\infty} \left[\psi_1^2 + \psi_2^2 - 4\sigma u_0 u_{\mu 0}(\psi_1^2 + \psi_1\psi_2 + \psi_2^2)\right] dx}{\int_{-\infty}^{\infty}(\psi_1\phi_1 - \psi_2\phi_2)dx} \tag{3.25}$$

and

$$\gamma = \frac{\sigma \int_{-\infty}^{\infty} \left\{ \begin{array}{l} \psi_1^4 + 4\psi_1^2\psi_2^2 + \psi_2^4 - 4\sigma u_0 h(\psi_1^2 + \psi_1\psi_2 + \psi_2^2) \\ -2\sigma u_0[\psi_1^2 g_1 + 2\psi_1\psi_2(g_1 + g_2) + \psi_2^2 g_2] \end{array} \right\} dx}{\int_{-\infty}^{\infty}(\psi_1\phi_1 - \psi_2\phi_2)dx}. \tag{3.26}$$

In view of (2.13) and our third assumption at the end of section 2, the above three constants are well defined. Dynamical equations (3.22)–(3.23) are our normal form for nonlinear wave dynamics near Hamiltonian–Hopf bifurcations in the PDE (2.1).

Of the three constants in this normal form, α and β are always real. But γ is real only when $2\omega < \mu_0$ and becomes complex if $2\omega > \mu_0$, since the functions (g_1, g_2) involved in the definition of γ are real and complex under those conditions, respectively (see earlier text in this section).

The physical meaning of parameter β in (3.23) can be revealed by considering small-B solutions. In this case, $\mu_{1T} \approx 0$, i.e., μ_1 is approximately a constant, and the resulting solution (3.1) is approximately a soliton with propagation constant $\mu \approx \mu_0 + \epsilon^2\mu_1$. The small perturbation B satisfies $B_{TT} - \beta\mu_1 B \approx 0$, and thus $B \sim e^{\tilde{\lambda}t}$, where $\tilde{\lambda} = \pm\epsilon\sqrt{\beta\mu_1}$. If $\beta\mu_1 < 0$, then the perturbation B is bounded, meaning that the soliton is before the Hamiltonian–Hopf bifurcation. When $\beta\mu_1 > 0$, the perturbation B exponentially grows, meaning that the soliton is after the Hamiltonian–Hopf bifurcation. In the latter case, recalling (3.5), we see that the quartet of complex eigenvalues born out of Hamiltonian–Hopf bifurcations is $\lambda \approx \pm i\omega \pm \sqrt{\beta(\mu - \mu_0)}$. Thus, physically β determines the growth rate of perturbations after Hamiltonian–Hopf bifurcations. We note that if one just wants to obtain this $\lambda(\mu)$ relation, then it is faster to perform a standard perturbation analysis on the linear-stability eigenvalue problem (2.5) around Hamiltonian–Hopf bifurcations (such eigenvalue calculations near other types of soliton bifurcations can be found in [20, 28]). However, our more elaborate multiscale perturbation analysis in this paper can achieve much more, and this $\lambda(\mu)$ relation is just a small by-product.

The normal form (3.22)–(3.23) can be further simplified. Notice that (3.22) can be integrated once, and we get

$$\mu_1 = \alpha|B|^2 + c_0, \tag{3.27}$$

where c_0 is a real constant which can be determined from the initial conditions of μ_1 and B. Substituting this equation into (3.23), we obtain a decoupled equation for B as

$$B_{TT} - \widehat{\beta}\, B + \widehat{\gamma}\, |B|^2 B = 0, \tag{3.28}$$

where

$$\widehat{\beta} = \beta\, c_0, \quad \widehat{\gamma} = \gamma - \alpha\beta. \tag{3.29}$$

In this equation, $\widehat{\beta}$ is a real constant, while $\widehat{\gamma}$ can be real or complex depending on the reality of γ. Equation (3.28) is a reduced normal form for nonlinear wave dynamics near Hamiltonian–Hopf bifurcations. This reduced normal form is a second-order nonlinear ODE for a complex variable B.

For a different symmetry-breaking bifurcation of solitons in the NLS equation with external potentials (2.1), a normal form similar to (3.28) was derived by Pelinovsky and Phan [17], but the variable and the nonlinear coefficient in their normal form were both real. For the present Hamiltonian–Hopf bifurcation, both the variable B and the nonlinear coefficient $\widehat{\gamma}$ can be complex, and this fact will have important consequences on the solution dynamics, as we will elaborate below.

4. Solution behaviors in the normal form. Now we analyze solution dynamics in the reduced normal form (3.28).

4.1. Solutions for real nonlinear coefficient $\widehat{\gamma}$. When $\widehat{\gamma}$ is real, (3.28) can be solved exactly. In polar variables $B = be^{i\xi}$, where b is the amplitude and ξ the phase of B, (3.28) yields

$$b_{TT} - \widehat{\beta} b + \widehat{\gamma} b^3 - \xi_T^2 b = 0, \tag{4.1}$$

$$(b^2 \xi_T)_T = 0. \tag{4.2}$$

The second equation shows that $b^2 \xi_T = w_0$, where w_0 is a real constant. Using this relation, (4.1) reduces to

$$b_{TT} - \widehat{\beta} b + \widehat{\gamma} b^3 - \frac{w_0^2}{b^3} = 0, \tag{4.3}$$

which describes the motion of a particle in a potential well,

$$b_{TT} + W'(b) = 0, \tag{4.4}$$

where the potential $W(b)$ is

$$W(b) = -\frac{1}{2}\widehat{\beta} b^2 + \frac{1}{4}\widehat{\gamma} b^4 + \frac{w_0^2}{2b^2}. \tag{4.5}$$

Then depending on system parameters $(\widehat{\beta}, \widehat{\gamma})$ and initial conditions, the solution $B(T)$ can be completely obtained.

A special but important class of solutions arises when $w_0 = 0$, i.e., $\xi_T = 0$. In view of gauge invariance, these solutions are equivalent to real-B solutions, which will be elaborated further below.

When B is real, (3.28) becomes

$$B_{TT} - \widehat{\beta} B + \widehat{\gamma} B^3 = 0. \tag{4.6}$$

The solution dynamics in this equation is best illustrated by its phase portrait in the (B, B_T) plane. Depending on the signs of $\widehat{\beta}$ and $\widehat{\gamma}$, four qualitatively different phase portraits are displayed in Figure 1. These phase portraits show that when $\widehat{\gamma} > 0$, the trajectories are all bounded and almost always periodic (see the left panels), which correspond to time-periodic bound states (3.1) in the PDE system (2.1). When $\widehat{\gamma} < 0$, trajectories all escape to infinity if $\widehat{\beta} > 0$ (upper right panel) and escape to infinity for larger initial conditions and stay bounded and periodic for smaller initial conditions if $\widehat{\beta} < 0$ (lower right panel).

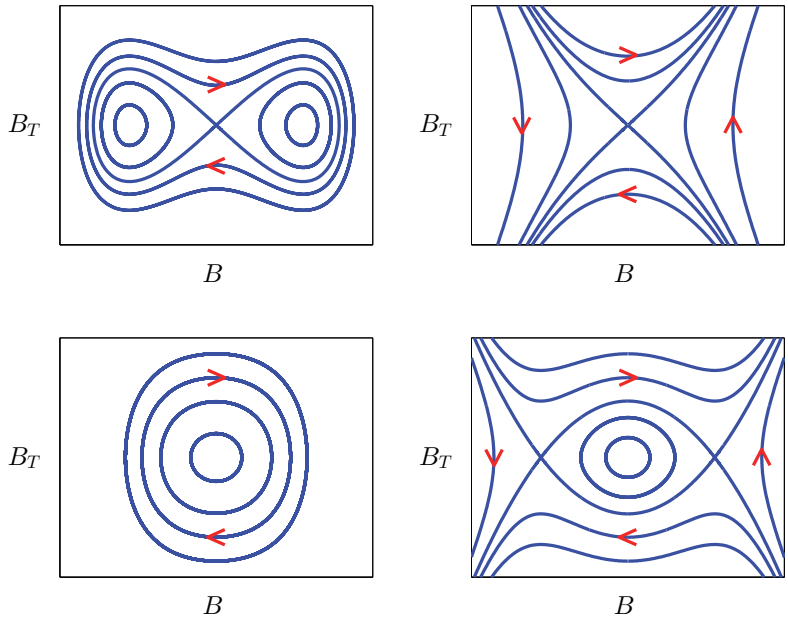

FIG. 1. *(Color online.) Phase portraits of the normal form* (3.28) *for real values of* $\widehat{\gamma}$ *and* B. *Upper left:* $\widehat{\beta} > 0, \widehat{\gamma} > 0$. *Upper right:* $\widehat{\beta} > 0, \widehat{\gamma} < 0$. *Lower left:* $\widehat{\beta} < 0, \widehat{\gamma} > 0$. *Lower right:* $\widehat{\beta} < 0, \widehat{\gamma} < 0$.

The phase portraits in Figure 1 are drawn for fixed model coefficients $\widehat{\beta}$, $\widehat{\gamma}$ and different initial conditions of (B, B_T). The reader may recall from (3.29) that $\widehat{\beta}$ is related to c_0, which depends on the initial condition of B in view of (3.27). As such, the reader might wonder if the phase portraits of Figure 1 are of any use if c_0 cannot be treated as fixed. There are two ways to look at this issue. One way is to fix c_0 first (hence, the phase portrait is known from Figure 1). Then for different initial conditions of B, we can choose the initial condition of μ_1 according to (3.27) as $\mu_{10} = \alpha|B_0|^2 + c_0$. Under this choice of μ_{10}, solution dynamics of $B(T)$ for different initial conditions would be described by the underlying phase portrait; in addition, every orbit in the phase portrait can be realized by a proper selection of the initial condition of B. The other way to look at this issue is to fix the initial conditions of B, B_T, and μ_1 now, corresponding to a given initial condition of the PDE (this is what we will do in the numerical examples of the next section). In this case, we can calculate c_0 from (3.27), and hence the phase portrait is ascertained from Figure 1. Then, since the initial conditions of B and B_T have been selected, we can read off the solution orbit of $B(T)$ from that phase portrait directly. From these two points of view, we see that the phase portraits in Figure 1 are indeed useful since they show us different types of solution behaviors for different initial conditions of B and μ_1.

4.2. Solutions for complex nonlinear coefficient $\widehat{\gamma}$. When $\widehat{\gamma}$ is complex, under polar variables $B = be^{i\xi}$ and the notation $w \equiv r^2\xi_T$, (3.28) becomes

$$b_{TT} - \widehat{\beta}\, b + \mathrm{Re}(\widehat{\gamma})\, b^3 - \frac{w^2}{b^3} = 0, \tag{4.7}$$

$$w_T = -\mathrm{Im}(\widehat{\gamma})\, b^4. \tag{4.8}$$

The first equation shows that b is bounded away from zero. Then the second shows that w keeps increasing or decreasing to infinity. Viewing (4.7) as the motion of a particle in a potential well, when w goes to infinity, the potential term $w^2/(2b^2)$ dominates, and hence the solution b escapes to infinity as well.

We can further determine precisely in which manner the solution (b, w) escapes to infinity. The nature of nonlinearity in (4.7)–(4.8) indicates that the solution will escape to infinity in finite time. Suppose the time of blowup is T_0, and

$$b(T) \sim \frac{b_1}{(T_0 - T)^m}, \quad w(T) \sim \frac{w_1}{(T_0 - T)^n}, \quad T \sim T_0, \tag{4.9}$$

where b_1, w_1, m, n are real constants to be determined. Substituting these asymptotics into (4.8), we get

$$n = 4m - 1, \quad w_1 = -\frac{\mathrm{Im}(\widehat{\gamma})\, b_1^4}{n}. \tag{4.10}$$

Substituting the asymptotics (4.9) and the above equation into (4.7) and using dominant balance, we get

$$m = 1, \quad 2b_1 + \mathrm{Re}(\widehat{\gamma})\, b_1^3 = \frac{w_1^2}{b_1^3}. \tag{4.11}$$

After solving (b_1, w_1) from the above two equations, we find that the blowup profile of the solution $B(T)$ is

$$b(T) \sim \frac{b_1}{T_0 - T}, \quad \xi(T) \sim c_1 \ln(T_0 - T), \quad T \sim T_0, \tag{4.12}$$

where

$$b_1 = \frac{3}{\sqrt{2}\,\mathrm{Im}(\widehat{\gamma})} \sqrt{\mathrm{Re}(\widehat{\gamma}) + \sqrt{[\mathrm{Re}(\widehat{\gamma})]^2 + \frac{8}{9}\,[\mathrm{Im}(\widehat{\gamma})]^2}} \tag{4.13}$$

and

$$c_1 = \frac{1}{3}\mathrm{Im}(\gamma)\, b_1^2. \tag{4.14}$$

Notice that this collapsing profile is completely determined by the nonlinear coefficient γ, except for the collapsing time T_0. Notice also that both the amplitude b and phase ξ collapse, but at different rates.

To illustrate these collapsing solutions for complex $\widehat{\gamma}$, we take $\widehat{\gamma} = 1 + i$ and two different values of ± 1 for $\widehat{\beta}$. For these parameter choices, we have computed (3.28) for various initial conditions and found that the solution always collapses, and the collapsing profile exactly matches that predicted by (4.12). Two examples of such computations are displayed in Figure 2 along with analytical collapsing profiles for comparison. For these two values of $\widehat{\beta}$, the two solutions $B(T)$ initially behave quite differently. But they both approach the same collapsing profile (4.12) in the end.

Collapsing solutions of $B(T)$ correspond to PDE solutions (3.1), where the Hopf oscillation mode (3.5) strongly intensifies and the underlying soliton $u_0(x)$ eventually breaks up. This solution collapse occurs when $\widehat{\gamma}$ is complex, i.e., when $2\omega > \mu_0$, where resonance with the continuous spectrum arises in the U_2 solution (3.8). Due to this

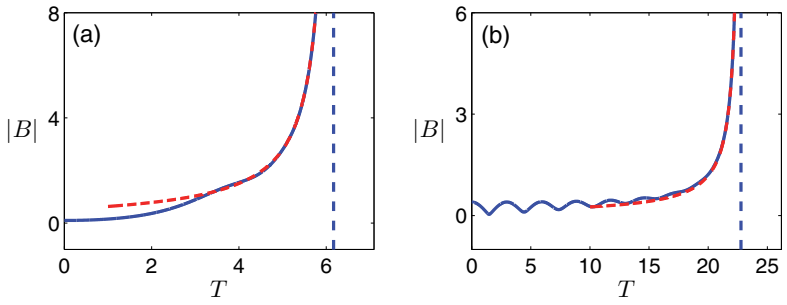

FIG. 2. *(Color online.) Collapsing solutions of the normal form* (3.28) *when* $\widehat{\gamma}$ *is complex.* (a) $\widehat{\beta} = 1$ *and* $\widehat{\gamma} = 1 + i$. (b) $\widehat{\beta} = -1$ *and* $\widehat{\gamma} = 1 + i$. *Solid blue lines are numerically obtained solutions of the normal form, dashed red lines are analytical collapsing profiles* (4.12)*, and vertical dashed lines are collapsing times.*

resonance, energy is channeled from the underlying soliton to the Hopf oscillation mode (3.5) and continuous-wave radiation. When $2\omega < \mu_0$, this resonance does not occur in U_2, $\widehat{\gamma}$ is real, and the ODE solution $B(T)$ can be bounded (see Figure 1). However, due to nonlinearity-induced higher harmonics, there always exists a higher harmonic $e^{in\omega}$ for some integer n so that $n\omega > \mu_0$, in which case resonance with the continuous spectrum will occur in the U_n solution of the perturbation expansion (3.1). As a consequence, when $2\omega < \mu_0$, the B solution is still expected to collapse, and the underlying soliton $u_0(x)$ is still expected to break up, except that these events will take much more time to develop since the resonance is at higher orders of the perturbation expansion.

Notice that the B solution can be viewed as a Hopf-mode perturbation to a soliton with the propagation constant $\mu \approx \mu_0 + \epsilon^2\mu_1$ near the Hamiltonian–Hopf bifurcation point, as seen from (3.1), (3.5), and (3.8). Since B always collapses (or is expected to collapse), regardless of how small it is initially and of what initial value μ_1 takes, our analysis then predicts that all solitons are unstable near the Hamiltonian–Hopf bifurcation point, regardless of whether they are above or below this bifurcation. The instability above the bifurcation is due to complex eigenvalues in the soliton's linear-stability spectrum, which appear after the collision of purely imaginary eigenvalues, and thus it is a linear spectral instability. The instability below the bifurcation, however, is a nonlinear instability, since all eigenvalues in the soliton's linear-stability spectrum are purely imaginary before the collision of imaginary eigenvalues, indicating that the soliton is spectrally stable. So we have here a case where solitons are spectrally (linearly) stable but nonlinearly unstable. Recall that before the Hamiltonian–Hopf bifurcation, the soliton's linear-stability spectrum contains purely imaginary eigenvalues of negative Krein signatures (whose collisions with eigenvalues of positive Krein signatures lead to this bifurcation [21, 23]). Thus, our results are consistent with those in [29], where it was shown that solitons with imaginary eigenvalues of negative Krein signatures are always nonlinearly unstable even if linearly stable. Then are there solitons in (2.1) that are nonlinearly stable? The answer is positive, but such solitons need to be ground states which bifurcate from the fundamental linear mode (i.e., the largest eigenvalue) of the potential, while solitons exhibiting Hamiltonian–Hopf bifurcations always bifurcate from the higher linear modes (i.e., excited states) of the potential. More will be said on this in the numerical examples below.

5. Numerical examples. In this section, we use several numerical examples to illustrate the theory and compare the numerical results with the normal form's predictions.

Example 1. In our first example, we take

$$V(x) = -3\left[\operatorname{sech}^2(x+1) + \operatorname{sech}^2(x-1)\right], \tag{5.1}$$

which is a symmetric double-well potential, and $\sigma = 1$ (focusing nonlinearity). This potential is displayed in Figure 3(a). This potential admits three linear discrete eigenvalues $\mu_a < \mu_b < \mu_c$, with the middle one being $\mu_b \approx 1.4104$. From this linear eigenmode, a family of dipole-type solitons bifurcates out. The reason for choosing this dipole-soliton family bifurcating from the middle linear eigenmode is that, at low amplitudes of these solitons, it can be readily shown that the linear-stability operator iL has two purely imaginary eigenvalues of opposite Krein signatures in the upper half plane. Specifically, one imaginary eigenvalue is approximately $i(\mu_c - \mu_b)$ and has negative Krein signature, and the other imaginary eigenvalue is approximately $i(\mu_b - \mu_a)$ and has positive Krein signature. The presence of these two imaginary eigenvalues of opposite Krein signatures makes Hamiltonian–Hopf bifurcation possible as the amplitude of the soliton increases (see section 2).

In Figure 3(d) the power curve of this soliton family is displayed. At two marked points of this power curve where $\mu = \mu_0 \pm 0.05$, profiles of the solitons are plotted in Figure 3(b),(c). Linear-stability spectra of these solitons are shown in Figure 3(e),(f). It is seen that for the lower-power soliton (see panel (b)), the spectrum is all-imaginary with a pair of discrete imaginary eigenvalues close to each other in the upper half plane (see panel (e)). This pair of imaginary eigenvalues originate from the eigenvalues $i(\mu_c - \mu_b)$ and $i(\mu_b - \mu_a)$ of zero-power solitons and thus have opposite Krein signatures. For the higher-power soliton (see panel (c)), this pair of discrete eigenvalues has collided and bifurcated off the imaginary axis, indicating that a Hamiltonian–Hopf bifurcation has occurred (see panel (f)). The exact location of this Hamiltonian–Hopf bifurcation is at $\mu_0 \approx 1.8572$, where the two discrete eigenvalues coalesce at $i\omega$, with $\omega \approx 1.3450$. Notice that $2\omega > \mu_0$; thus γ is complex. Numerical values for constants α, β, and γ in the normal form (3.22)–(3.23) are computed from numerical solutions of u_0, $\psi_{1,2}$, $\phi_{1,2}$ and the formulae (3.24)–(3.26) as

$$\alpha \approx 0.2660, \quad \beta \approx 0.0476, \quad \gamma \approx 0.0780 + 0.0144i. \tag{5.2}$$

In obtaining these numbers, the eigenfunction $[\psi_1, \psi_2]^T$ is normalized so that the maximum of $\psi_1^2 + \psi_2^2$ is one.

Now we numerically investigate the dynamics of solutions near this Hamiltonian–Hopf bifurcation point. Numerical evolutions are performed by the pseudospectral method on a wide spatial interval, with damping conditions near the boundaries [26]. First, we consider dynamics above the bifurcation. For this purpose, we take the initial condition of the PDE as a perturbation of the unstable soliton in Figure 3(c) by Hopf oscillation mode (3.5), corresponding to $\epsilon^2 \mu_1|_{t=0} = 0.05$, $\epsilon B|_{t=0} = 0.01$, and $\epsilon^2 B_T|_{t=0} = 0$ in the perturbation solution (3.1). Whole-field evolution of this initial condition is illustrated in Figure 4(a), and the amplitude evolution at $x = 1.2$ is shown in Figure 4(b). It is seen that the underlying soliton breaks up and the solution evolves into oscillations which grow stronger over time. Taking the initial condition of the normal form (3.28) corresponding to the above initial condition of the PDE, the solution B of the normal form is plotted in Figure 4(c). This B solution grows and eventually blows up in finite time (the blowup part is not shown since the

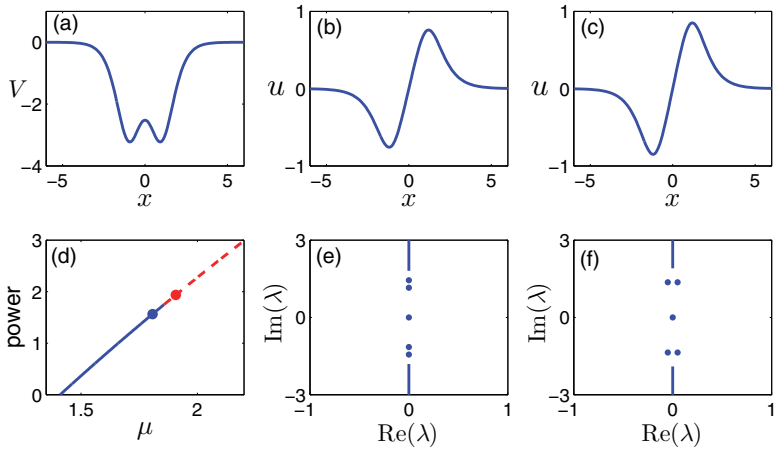

FIG. 3. *(Color online.) Solitons and their stability spectra in Example* 1. (a) *The double-well potential* (5.1). (b),(c) *Profiles of dipole solitons at the marked blue and red points of the power curve in* (d), *respectively; blue in the power curve represents stable solitons, and red represents unstable solitons.* (e),(f) *Linear-stability spectra of the solitons in* (b),(c), *respectively.*

perturbation theory will be invalid when the blowup occurs). Using this B solution, we have reconstructed the perturbation solution (3.1) (up to order ϵ^2), and the amplitude evolution at $x = 1.2$ is shown in Figure 4(d). Comparing this analytically reconstructed amplitude evolution with the numerical one in panel (b), we can see that the normal form (3.28) gives a good qualitative and quantitative prediction of the PDE dynamics above Hamiltonian–Hopf bifurcations over a long period of time.

Next we consider solution dynamics in Example 1 below the Hamiltonian–Hopf bifurcation. For this purpose, we take the initial condition of the PDE as a perturbation of the stable soliton in Figure 3(b) by Hopf oscillation mode (3.5), corresponding to $\epsilon^2\mu_1|_{t=0} = -0.05$, $\epsilon B|_{t=0} = 0.08$, and $\epsilon^2 B_T|_{t=0} = 0$ in the perturbation solution (3.1). Evolution of this initial condition is illustrated in Figure 5(a),(b),(c). It is seen that the soliton also eventually breaks up due to growing oscillations. This instability is interesting since the underlying soliton is linearly stable (see Figure 3(e)). Thus, this instability is a nonlinear instability. The analytical reason for this nonlinear instability is that the nonlinear coefficient $\widehat{\gamma}$ in the normal form (3.28) is complex (see (5.2)), and thus the ODE solution B always collapses both below and above the Hamiltonian–Hopf bifurcation (see Figure 2). From the ODE solution of the normal form (3.28), we have also reconstructed the perturbation solution (3.1), and the amplitude evolution at $x = 1.2$ is shown Figure 5(d). In this case, the normal form also gives a good qualitative and quantitative prediction of the PDE dynamics over long times.

It should be noted that even though solitons in Example 1 break up both below and above the Hamiltonian–Hopf bifurcation, this breakup occurs much more quickly above the bifurcation point since the soliton in this case is linearly unstable.

Example 2. Our second example pertains to the case where, at the Hamiltonian–Hopf bifurcation point, $2\omega < \mu_0$; hence γ is real. In this example, we take

$$V(x) = -3\left[\operatorname{sech}^2(x + 1.25) + \operatorname{sech}^2(x - 1.25)\right], \tag{5.3}$$

which is a slightly further-separated double-well potential (shown in Figure 6(a)),

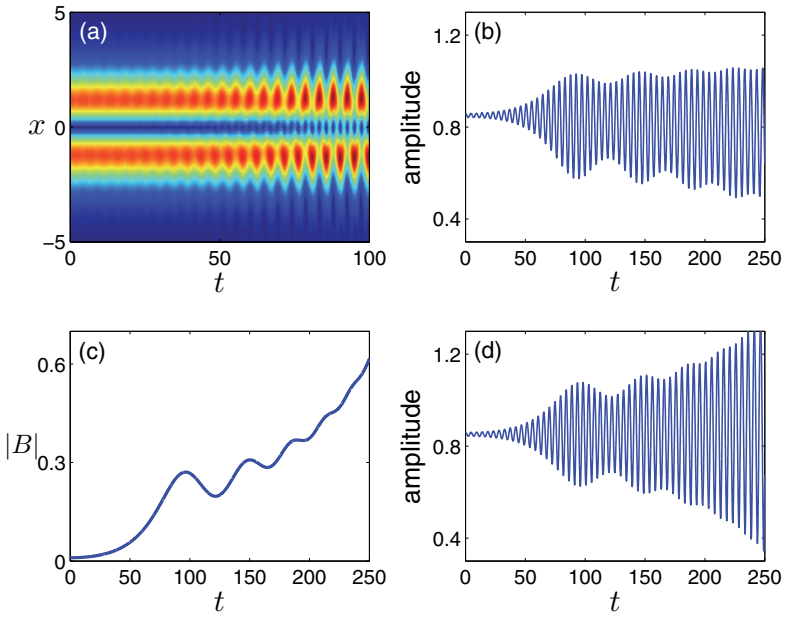

FIG. 4. *(Color online.) Solution evolution above Hamiltonian–Hopf bifurcation in Example* 1. (a) *Contour plot of the PDE solution in the* (x,t) *plane.* (b) *Amplitude evolution of the PDE solution versus time. Here the amplitude is measured as* $|U(x,t)|$ *at location* $x = 1.2$. (c) *The solution* $|B|$ *obtained from the normal form* (3.28). (d) *Amplitude evolution of the analytically reconstructed perturbation solution* (3.1).

and $\sigma = 1$ (focusing nonlinearity). This linear potential also admits three discrete eigenvalues, and the power curve of dipole-type solitons bifurcating from the middle eigenmode is plotted in Figure 6(b). At the propagation constant $\mu_0 \approx 3.5562$, a Hamiltonian–Hopf bifurcation occurs, and the coalesced eigenvalues on the imaginary axis are $i\omega$, where $\omega \approx 1.5559$. Notice that $2\omega < \mu_0$, and thus resonance does not occur in the U_2 solution, and γ is real in the normal form (3.22)–(3.23). Specifically, the constants in the normal form for this second example are

$$\alpha \approx 0.0372, \quad \beta \approx 0.0263, \quad \gamma \approx 0.2763, \tag{5.4}$$

where the eigenfunction $[\psi_1, \psi_2]^T$ is normalized to have unit maximum in $\psi_1^2 + \psi_2^2$. In this case, $\widehat{\gamma} = \gamma - \alpha\beta > 0$, and thus solutions of the normal form (3.28) are periodic (see Figure 1).

Figure 6(c) shows the linear-stability spectrum of the soliton at the propagation constant $\mu = \mu_0 + 0.05$ (marked by a red dot in Figure 6(b)). The presence of a quartet of complex eigenvalues in this spectrum signals that this soliton is above the Hamiltonian–Hopf bifurcation point.

Now we perturb this unstable soliton by Hopf oscillation mode (3.5), corresponding to $\epsilon^2\mu_1|_{t=0} = 0.05$, $\epsilon B|_{t=0} = 0.01$, and $\epsilon^2 B_T|_{t=0} = 0$ in the perturbation solution (3.1). The initial evolution of this perturbed state is shown in Figure 6(d), where the instability is seen to develop. Longer-time amplitude evolution of this perturbed state is plotted in Figure 7(a), where the amplitude of the solution is measured as $|U(x,t)|$ at location $x = 1.35$. It is seen that the envelope of this amplitude evolves quasi-periodically over a long time, but gradually loses its periodicity in analogy with that in Figure 5(c) for Example 1. Comparatively, the amplitude evolution of analytically

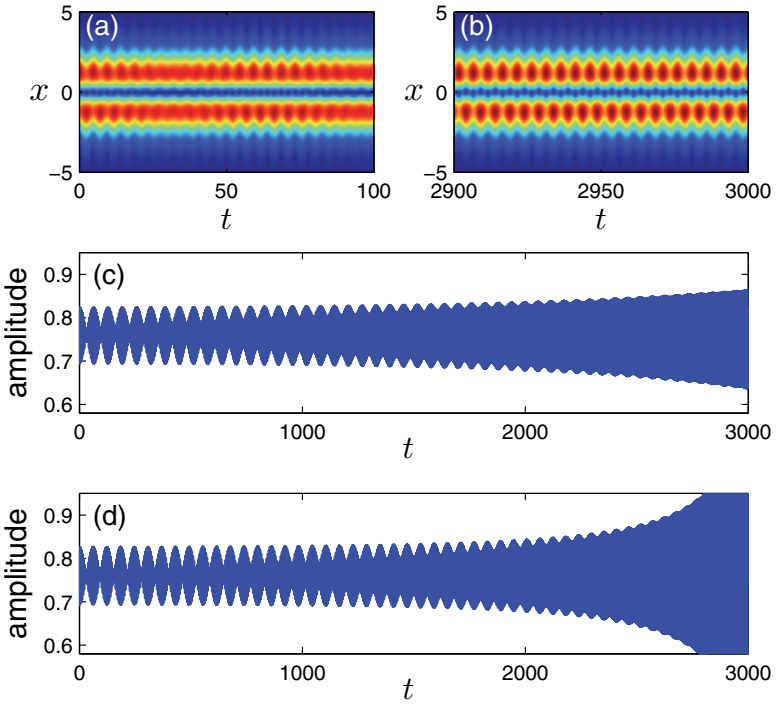

FIG. 5. *(Color online.) Solution evolution below Hamiltonian–Hopf bifurcation in Example* 1. (a),(b) *Contour plots of the PDE solution in the* (x,t) *plane on smaller and larger time intervals.* (c) *Amplitude evolution of the PDE solution versus time, where the amplitude is measured as* $|U(x,t)|$ *at location* $x = 1.2$. (d) *Amplitude evolution of the analytically reconstructed perturbation solution* (3.1). *In* (c),(d), *seemingly solid blue regions actually are made up of very fast oscillations as in Figure* 4(b),(d).

reconstructed perturbation solution (3.1) is displayed in Figure 7(b). The envelope of this analytical amplitude evolution is periodic, because for this second example, $\widehat{\gamma}$ is real, $\widehat{\beta} > 0$, and $\widehat{\gamma} > 0$, and hence the normal form's solutions are periodic (see Figure 1 (upper left panel)). The numerical and analytical amplitude evolutions in Figure 7 are in good agreement over long times (on the order of hundreds of time units). Their difference over very long times (on the order of thousands of time units) is due to the fact that for the present parameters, $3\omega > \mu_0$, and thus resonance with the continuous spectrum will occur in the U_3 solution, and this resonance will break the periodic oscillation. But our perturbation theory and the resulting normal form do not account for resonance at such high orders.

In the two examples above, potentials $V(x)$ were both symmetric and double-well. In our third example below, we choose a potential which is neither symmetric nor double-well.

Example 3. In this third example, we take

$$V(x) = -2\left\{\tanh[2(x+3)] - \tanh[0.5(x-3)]\right\}, \tag{5.5}$$

which is an asymmetric single-well potential; see Figure 8(a). This potential admits four linear discrete eigenvalues. From its second eigenmode, a family of dipole-type solitons bifurcate out under focusing nonlinearity ($\sigma = 1$). At $\mu_0 \approx 2.8426$ of this

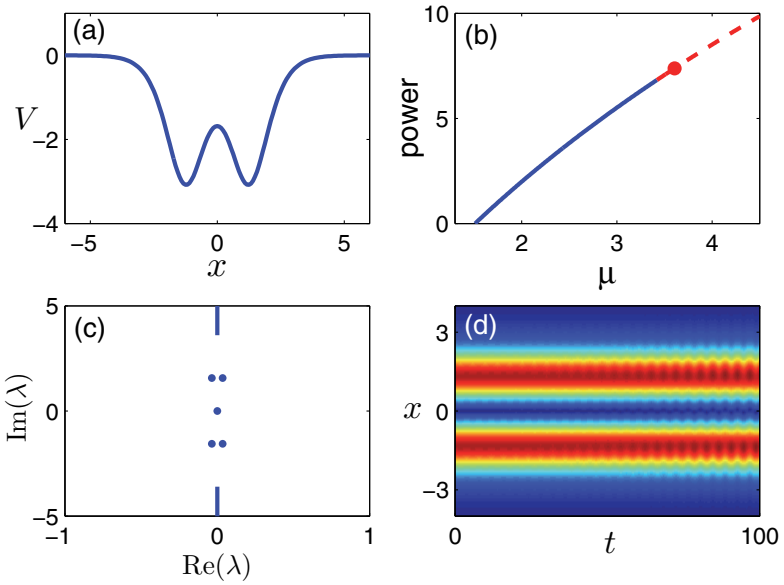

FIG. 6. *(Color online.)* (a) *The double-well potential* (5.3) *in Example* 2. (b) *Power curve of dipole-solitons in this potential, where blue indicates stable solitons, and red indicates unstable ones.* (c) *Linear-stability spectrum of the unstable soliton marked by a red dot in panel* (b). (d) *Initial evolution of the unstable soliton at the red dot of panel* (b) *under perturbations.*

soliton family, a Hamiltonian–Hopf bifurcation occurs, and the coalesced eigenvalues on the imaginary axis are $i\omega$, where $\omega \approx 0.9102$. The constants in the normal form are now $\alpha \approx 0.3572$, $\beta \approx 0.0279$, and $\gamma \approx 0.0386$.

At the propagation constant $\mu = \mu_0 + 0.01$, the soliton is linearly unstable since it is above the Hamiltonian–Hopf bifurcation point. Now we perturb this soliton by Hopf oscillation mode (3.5), corresponding to $\epsilon^2 \mu_1|_{t=0} = 0.01$, $\epsilon B|_{t=0} = 0.02$, and $\epsilon^2 B_T|_{t=0} = 0$ in the perturbation solution (3.1). Evolution of this perturbed state is shown in Figure 8(b), where the instability is seen to develop. Longer-time amplitude evolution of this perturbed state is plotted in Figure 8(c). It is seen that the envelope of this amplitude first increases due to Hopf instability. But this increase later saturates, and then it starts to decrease. This pattern repeats for long times (but eventually breaks up as in Figure 7(a)). For comparison, amplitude evolution of the analytically reconstructed perturbation solution (3.1) is displayed in Figure 8(d), and good agreement with Figure 8(c) can be observed.

6. Summary and discussion. In this paper, we have derived a normal form for general Hamiltonian–Hopf bifurcations of solitons in NLS equations with external potentials. This normal form is a simple second-order nonlinear ODE whose dynamics is analytically predictable, and it is asymptotically accurate in describing solution dynamics near Hamiltonian–Hopf bifurcations. We showed that when the nonlinear coefficient in this normal form is complex, which occurs if the second harmonic of the Hopf bifurcation frequency is resonant with the continuous spectrum of the system, the solution of this normal form blows up to infinity in finite time, indicating that solution oscillations near Hamiltonian–Hopf bifurcations will strongly amplify and eventually be destroyed. When the nonlinear coefficient of the normal form is

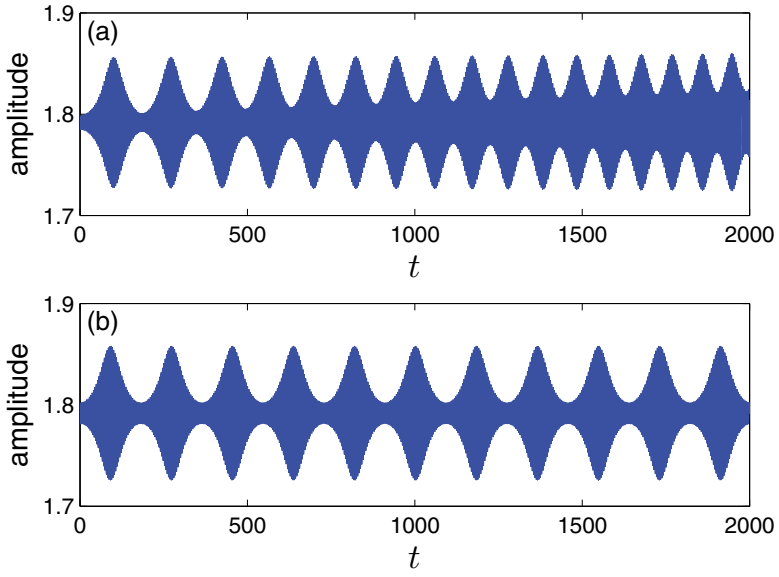

FIG. 7. *(Color online.)* (a) *Amplitude evolution of the PDE solution for the perturbed soliton in Figure* 6(d) *over longer times in Example* 2. (b) *Amplitude evolution of the analytically reconstructed perturbation solution* (3.1).

real, the normal form can admit periodic solutions, which correspond to long-lasting solution oscillations in the original PDE system. A quantitative comparison between the normal form's predictions and true PDE solutions was also made in several numerical examples, and good agreement was obtained. The normal form we derived sheds much light on the analytical understanding of solution behaviors around general Hamiltonian–Hopf bifurcations.

It is noted that even though the normal form in this paper was derived for the specific NLS equation (2.1) with cubic nonlinearity and linear potentials, the same calculation can be trivially extended to generalized NLS equations with arbitrary forms of nonlinearities and potentials (including nonlinear potentials) [19]. Thus, the normal form we derived is valid for Hamiltonian–Hopf bifurcations in all generalized nonlinear Schrödinger equations.

It is interesting to note that our normal form can be dissipative (since its nonlinear coefficient can be complex), even though the original PDE system (2.1) is conservative. This dissipative nature of the normal form is caused by resonant radiation emission from nonlinearity-induced higher harmonics of oscillating modes. However, this resonant radiation emission does not lead to the decay of solution oscillations. Instead, solution oscillations intensity, as the normal form predicts and the numerics confirms. This situation is analogous to oscillations induced by an internal mode with negative Krein signature [29].

Lastly, we would like to point out that our normal form does not admit chaotic solutions, which indicates that solution dynamics near Hamiltonian–Hopf bifurcations is not chaotic in the PDE system (at least on the time scale of ϵ^{-1} for which the normal form was derived). This analytical prediction is consistent with our numerical PDE results. In the NLS equation with a triple-well potential studied in [15], chaotic motion was reported in both the ODE model and PDE system. In that case, the

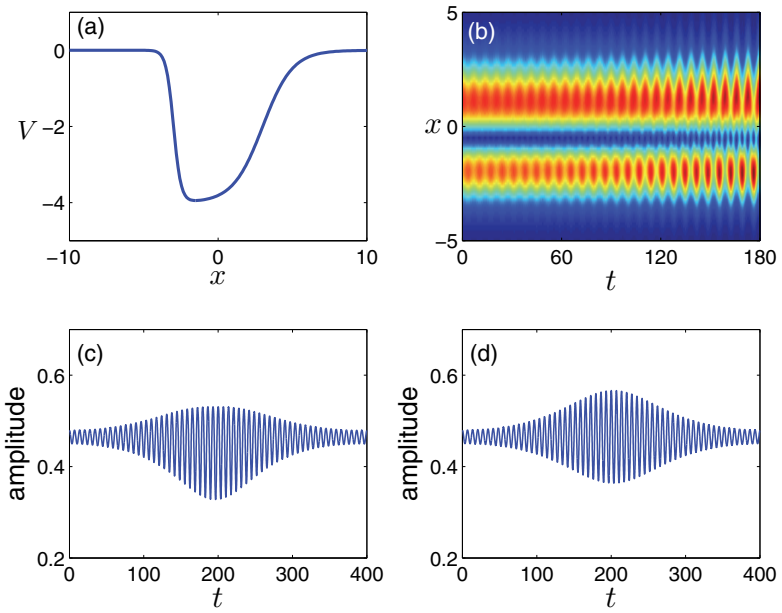

FIG. 8. *(Color online.)* (a) *The asymmetric potential* (5.5) *in Example* 3. (b) *Evolution of the unstable soliton with* $\mu = \mu_0 + 0.01$ *under perturbations.* (c) *Amplitude evolution of the PDE solution.* (d) *Amplitude evolution of the analytically reconstructed perturbation solution* (3.1).

Hamiltonian–Hopf bifurcation occurred at low powers of solitons, where the chaotic motion was very weak in the ODE model (if at all). Notice that the ODE model derived in [15] did not account for resonant radiation emission of oscillating solutions, and thus in the PDE system where such resonant radiation is present, weak chaotic motion of the ODE model may not materialize. Whether there is chaotic motion near Hamiltonian–Hopf bifurcations in the PDE system, on time scales much longer than $O(\epsilon^{-1})$, is a question which may merit further investigation.

REFERENCES

[1] G. NICOLIS AND J.F.G. AUCHMUTY, *Dissipative structures, catastrophes, and pattern formation: A bifurcation analysis*, Proc. Natl. Acad. Sci. USA, 71 (1974), pp. 2748–2751.

[2] J.F.G. AUCHMUTY AND G. NICOLIS, *Bifurcation analysis of reaction–diffusion equations*—III. *Chemical oscillations*, Bull. Math. Biol., 38 (1976), pp. 325–350.

[3] R.J. DEISSLER AND H.R. BRAND, *Periodic, quasiperiodic, and chaotic localized solutions of the quintic complex Ginzburg–Landau equation*, Phys. Rev. Lett., 72 (1994), pp. 478–481.

[4] A. ANKIEWICZA, N. AKHMEDIEVA, AND J.M. SOTO-CRESPO, *Novel bifurcation phenomena for solitons in nonlinear saturable couplers*, Opt. Commun., 116 (1995), pp. 411–415.

[5] B. BUFFONI, A.R. CHAMPNEYS, AND J.F. TOLAND, *Bifurcation and coalescence of a plethora of homoclinic orbits for a Hamiltonian system*, J. Dyn. Differential Equations, 8 (1996), pp. 221–279.

[6] T.S. YANG AND T.R. AKYLAS, *On asymmetric gravity-capillary solitary waves*, J. Fluid Mech., 330 (1997), pp. 215–232.

[7] A.V. GETLING, *Rayleigh-Bénard Convection: Structures and Dynamics*, World Scientific, Singapore, 1998.

[8] A.M. RUCKLIDGE, M. SILBER, AND J. FINEBERG, *Secondary instabilities of hexagons: A bifurcation analysis of experimentally observed Faraday wave patterns*, in Bifurcations, Symmetry and Patterns, J. Buescu, S. Castro, A.P. Dias, and I. Labouriau, eds., Birkhäuser Verlag, Basel, Switzerland, 2002, pp. 101–114.

[9] P.G. Kevrekidis, Z. Chen, B.A. Malomed, D.J. Frantzeskakis, and M.I. Weinstein, *Spontaneous symmetry breaking in photonic lattices: Theory and experiment*, Phys. Lett. A, 340 (2005), pp. 275–280.
[10] T. Kapitula, P.G. Kevrekidis, and Z. Chen, *Three is a crowd: Solitary waves in photorefractive media with three potential wells*, SIAM J. Appl. Dyn. Syst., 5 (2006), pp. 598–633.
[11] E.W. Kirr, P.G. Kevrekidis, E. Shlizerman, and M.I. Weinstein, *Symmetry-breaking bifurcation in nonlinear Schrödinger/Gross–Pitaevskii equations*, SIAM J. Math. Anal., 40 (2008), pp. 566–604.
[12] C. Wang, G. Theocharis, P.G. Kevrekidis, N. Whitaker, K.J.H. Law, D.J. Frantzeskakis, and B.A. Malomed, *Two-dimensional paradigm for symmetry breaking: The nonlinear Schrödinger equation with a four-well potential*, Phys. Rev. E, 80 (2009), 046611.
[13] J.L. Marzuola and M.I. Weinstein, *Long time dynamics near the symmetry breaking bifurcation for nonlinear Schrödinger/Gross-Pitaevskii equations*, Discrete Contin. Dyn. Syst. A, 28 (2010), pp. 1505–1554.
[14] E.W. Kirr, P.G. Kevrekidis, and D.E. Pelinovsky, *Symmetry-breaking bifurcation in the nonlinear Schrodinger equation with symmetric potentials*, Commun. Math. Phys., 308 (2011), pp. 795–844.
[15] R.H. Goodman, *Hamiltonian Hopf bifurcations and dynamics of NLS/GP standing-wave modes*, J. Phys. A, 44 (2011), 425101.
[16] H.C. Kao and E. Knobloch, *Weakly subcritical stationary patterns. Eckhaus instability and homoclinic snaking*, Phys. Rev. E, 85 (2012), 026211.
[17] D.E. Pelinovsky and T. Phan, *Normal form for the symmetry-breaking bifurcation in the nonlinear Schrodinger equation*, J. Differential Equations, 253 (2012), pp. 2796–2824.
[18] J. Yang, *No stability switching at saddle-node bifurcations of solitary waves in generalized nonlinear Schroedinger equations*, Phys. Rev. E, 85 (2012), 037602.
[19] J. Yang, *Classification of solitary wave bifurcations in generalized nonlinear Schrödinger equations*, Stud. Appl. Math., 129 (2012), pp. 133–162.
[20] J. Yang, *Stability analysis for pitchfork bifurcations of solitary waves in generalized nonlinear Schroedinger equations*, Phys. D, 244 (2013), pp. 50–67.
[21] R.S. MacKay, *Stability of equilibria of Hamiltonian systems*, in Hamiltonian Dynamical Systems, R.S. MacKay and J. Meiss, eds., Adam Hilger, Bristol, 1987, pp. 137–153.
[22] D.E. Pelinovsky, *Localization in Periodic Potentials: From Schrödinger Operators to the Gross-Pitaevskii Equation*, London Math. Soc. Lecture Note Ser. 390, Cambridge University Press, Cambridge, UK, 2011.
[23] T. Kapitula and K. Promislow, *Spectral and Dynamical Stability of Nonlinear Waves*, Springer, Berlin, 2013.
[24] Y.S. Kivshar and G.P. Agrawal, *Optical Solitons: From Fibers to Photonic Crystals*, Academic Press, San Diego, 2003.
[25] L.P. Pitaevskii and S. Stringari, *Bose-Einstein Condensation*, Oxford University Press, Oxford, UK, 2003.
[26] J. Yang, *Nonlinear Waves in Integrable and Nonintegrable Systems*, Math. Model. Comput. 16, SIAM, Philadelphia, 2010.
[27] D.E. Pelinovsky and J. Yang, *A normal form for nonlinear resonance of embedded solitons*, R. Soc. Lond. Proc. Ser. A Math. Phys. Eng. Sci., 458 (2002), pp. 1469–1497.
[28] J. Yang, *Stability switching at transcritical bifurcations of solitary waves in generalized nonlinear Schrödinger equations*, Phys. Lett. A, 377 (2013), pp. 866–870.
[29] P.G. Kevrekidis, D.E. Pelinovsky, and A. Saxena, *When linear stability does not exclude nonlinear instability*, Phys. Rev. Lett., 114 (2015), 214101.